PERGAMON

International Journal of Heat and Mass Transfer 43 (2000) 147–159

International Journal of HEAT and MASS TRANSFER

www.elsevier.com/locate/ijhmt

Effect of disuniformities in vapor saturation pressure and coolant velocity on vapor back flow phenomena in single-pass air-cooled condensers

Giampietro Fabbri*

University of Bologna, D.I.E.N.C.A., Energie Engineering, Via Zannoni 45/2, 40134 Bologna, Italy

Received 2 November 1998; received in revised form 19 March 1999

Abstract

In the present work vapor back flow phenomena in single-pass, multiple-row, cross-flow air-cooled condensers are investigated. The condensation in this kind of heat exchangers is studied with the help of a mathematical model, which considers the effect of changes in the saturation temperature inside the tubes and changes in the air velocity in the direction transversal to the coolant flow. The model equations are solved with a new algorithm. The vapor distribution, the pressure drop between the inlet and outlet plena and the global effectiveness are determined under different working conditions. © 1999 Elsevier Science Ltd. All rights reserved.

Keywords: Condensation; Heat exchangers; Two-phase

1. Introduction

The performances of single-pass, multiple-row, cross-flow, air-cooled condensers [1,2] are often affected by vapor back flow phenomena. These phenomena occur when inlet and outlet plena are common for all tube rows and are responsible for the accumulation of noncondensable gases which, in practical applications, contaminate the vapor supplying the condensers. Noncondensable contaminant accumulation noticeably modify the performances of condensers and reduce the global effectiveness.

Vapor back flow and noncondensable contaminant accumulation phenomena have been analyzed by Berg and Berg [3] in single-pass, cross-flow, air-cooled condensers with a maximum of four tube rows. The analysis was limited to the case of isothermal condensation by neglecting changes in saturation temperature which are due to the pressure variation along the tubes. Moreover, a uniform velocity distribution was assumed in the air. Upon these hypotheses, the vapor distribution in the condenser rows was determined as a function of the row effectiveness which was assumed equal for all rows. Furthermore, for the limit case of row effectiveness equal to 1, the noncondensable contaminant accumulation was analyzed. Upon the same hypotheses, the Berg and Berg analysis of the noncondensable contaminant accumulation was extended by Breber et al. [4] to the case of the row effectiveness ranging from 0 to 1. Recently, the isothermal condensation of vapor either containing noncondensable gases or being free from them was analyzed in tubular heat exchangers with as high a number as desired of rows having different effectiveness [5–7].

In the present work we extend the previous analyses

* Tel.: +39-51-61-44516; fax: +39-51-61-44516.
E-mail address: giampietro.fabbri@mail.ing.unibo.it (G. Fabbri)

0017-9310/00/$ - see front matter © 1999 Elsevier Science Ltd. All rights reserved.
PII: S0017-9310(99)00124-6

Nomenclature

a_n	length of forward flow segment in the nth row (m)
A	saturation temperature sensitivity to changes in the pressure
B	air velocity profile parameter
C	row effectiveness sensitivity to changes in the air velocity
c_p	specific heat of the air (J/kg K)
E_g	global effectiveness of the condenser
E_n	effectiveness of the nth row
H	width of the section crossed by the air (m)
k_n	friction factor of the nth row (kg^{-1} s^{-2})
L	length of the tubes (m)
N	number of rows of the condenser
p_n	vapor pressure in the nth row (Pa)
T_n	air temperature before crossing the nth row (K)
T_{sn}	vapor saturation temperature in the nth row (K)
v_n	velocity of the air crossing the nth row (m/s)
w_n	vapor condensation rate per unit of tube length in the nth row (kg/m s)
w_0	reference vapor condensation rate per unit of tube length (kg/m s)
W_n	vapor flow rate in the nth row (kg/s)
x	parallel to tubes coordinate (m)
y	normalized parallel to tubes coordinate
α_n	normalized length of the forward flow segment of the nth row
γ_n	normalized friction factor of the nth row
θ_n	normalized air temperature before crossing the nth row
θ_{sn}	normalized vapor saturation temperature in the nth row
λ	latent heat of vaporization (J/kg)
ψ_n	normalized depression in the nth row referred to the inlet plenum pressure
Ψ	normalized pressure drop between inlet and outlet plena
ρ	density of the air (kg/m^3)
ϕ_n	normalized vapor flow rate in the nth row
ω_n	normalized velocity of the air crossing the nth row
$\hat{o}$	averaged value along the tubes
$\bar{o}$	velocity weighed average value along the tubes

of back flow phenomena in single-pass, cross-flow, air-cooled condensers by considering the effect of changes in the vapor saturation pressure inside the tubes and the effect of coolant velocity disuniformities. An original mathematical model is presented, which allows the vapor distribution to be determined in condensers with as many rows as desired with varying effectivenesses and different friction factors. A simple and fast calculation algorithm is proposed to solve the model equations. The vapor distribution, the pressure drop between the inlet and outlet plena and the global effectiveness are determined in different situations.

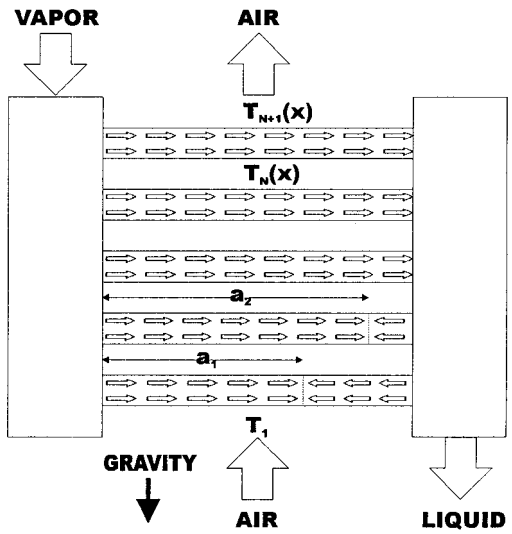

Fig. 1. Vapor back flow in a multiple-row, single-pass, cross-flow condenser.

2. The mathematical model

Let us consider a single-pass, cross-flow, air-cooled condenser, composed of N rows of horizontal tubes, with common inlet and outlet plena (Fig. 1). Let us introduce the following hypotheses:

- the vapor entering the condenser is free from non-condensable contaminants and entirely condenses inside;
- the pressure drops at both ends of the tubes and the pressure changes induced by deceleration are negligible;
- the heat exchanged by the superheated vapor and the condensate is negligible with respect to the heat lost in condensation;
- the heat transferred through the air in the perpen-

dicular to flow direction is negligible with respect to the heat exchanged between the tubes and the air.

In practical applications, the vapor is often contaminated by noncondensable gases. Their presence reduces the vapor pressure and the global heat transfer coefficient between the vapor and the air. As a consequence, the condenser tube effectiveness is reduced. Moreover, if vapor back flow occurs, after an initial phase, the noncondensable gases accumulate at the end of some tubes and noticeably reduce the global effectiveness of the condenser. However, vapor back flow phenomena, which occur at the beginning of the functioning of the condenser and are responsible for the contaminant accumulation in the subsequent phase, can be investigated by assuming a reduced effectiveness and ignoring noncondensable gases.

If the vapor which enters into a row does not entirely condense, it recirculates into other rows, through the outlet plenum (if a good drainage is ensured). This occurs because in some rows the pressure is lower than in the outlet plenum. Since the condensate flows out along the bottom of the tubes due to the gravity, internal pressure changes along the tubes are only induced by the vapor flow. The vapor saturation temperature consequently changes. Along the tubes in which vapor enters from both ends, the internal pressure decreases in the forward flow segment and increases in the back flow segment, passing through a minimum value (at $x = a_n$).

The vapor condensation rate per unit of tube length for the nth row can be calculated as:

$$w_n(x) = \frac{v_n(x) H \rho c_p}{\lambda} [T_{n+1}(x) - T_n(x)] \tag{1}$$

x being a parallel to tubes coordinate whose origin occurs at the beginning of the tubes, $v_n(x)$ the velocity of the air crossing the nth row, H the width of the section crossed by the air, ρ and c_p the density and specific heat of the air, respectively, λ the latent heat of vaporization, and $T_n(x)$ and $T_{n+1}(x)$ the temperatures of the air before and after crossing the nth row. By introducing in Eq. (1) the row effectiveness E_n:

$$E_n(x) = \frac{T_{n+1}(x) - T_n(x)}{T_{sn}(x) - T_n(x)} \tag{2}$$

the derivative of the vapor flow rate in the nth row, W_n, can be written as follows:

$$\frac{dW_n}{dx} = -w_n(x) = -\frac{v_n(x) H \rho c_p}{\lambda} E_n [T_{sn}(x) - T_n(x)] \tag{3}$$

where $T_{sn}(x)$ is the vapor saturation temperature, which is a function of the internal pressure of the nth tube. The following linearized relationship can be assumed between the saturation temperature and the pressure [8]:

$$T_{sn}(x) = T_{sn}(0) + k_s [p_n(x) - p_n(0)] \tag{4}$$

Since the inlet plenum is common, the saturation temperature at the beginning of the tubes $T_{sn}(0)$ is the same for every row. Lastly, the pressure drop per unit of tube length can be assumed proportional to the square of the vapor flow [3]:

$$\frac{dp_n}{dx} = \begin{cases} -k_n W_n^2 & \text{for } W_n > 0 \\ +k_n W_n^2 & \text{for } W_n \le 0 \end{cases} \tag{5}$$

where k_n is a friction factor which can assume a different value for each row, depending on the kind of the tubes (e.g. smooth, corrugated or finned [9–11]).

To obtain the vapor, pressure and temperature distributions in a dimensionless form, let us introduce the following dimensionless variables and parameters:

$$y = \frac{x}{L} \tag{6}$$

$$\phi_n = \frac{W_n}{w_0 L} \tag{7}$$

$$\psi_n = \frac{3[p_n(0) - p_n(Ly)]}{k_0 w_0^2 L^3} \tag{8}$$

$$\theta_n = \frac{T_n(Ly) - T_1}{T_{sn}(0) - T_1} \tag{9}$$

$$\theta_{sn} = \frac{T_{sn}(Ly) - T_1}{T_{sn}(0) - T_1} \tag{10}$$

$$\omega_n = \frac{v_n(Ly)}{\hat{v}} \tag{11}$$

$$\gamma_n = \frac{k_n}{k_0} \tag{12}$$

$$A = \frac{k_s k_0 w_0^2 L^3}{3[T_{sn}(0) - T_1]} \tag{13}$$

where L is the tube length, $\hat{v}$ the average air velocity, k_0 a reference value, and:

$$w_0 = \frac{\hat{v} H \rho c_p}{\lambda} [T_{sn}(0) - T_1] \tag{14}$$

From Eqs. (2), (4) and (5) it is then obtained:

$$\frac{d\phi_n}{dy} = -\omega_n E_n (\theta_{sn} - \theta_n) \tag{15}$$

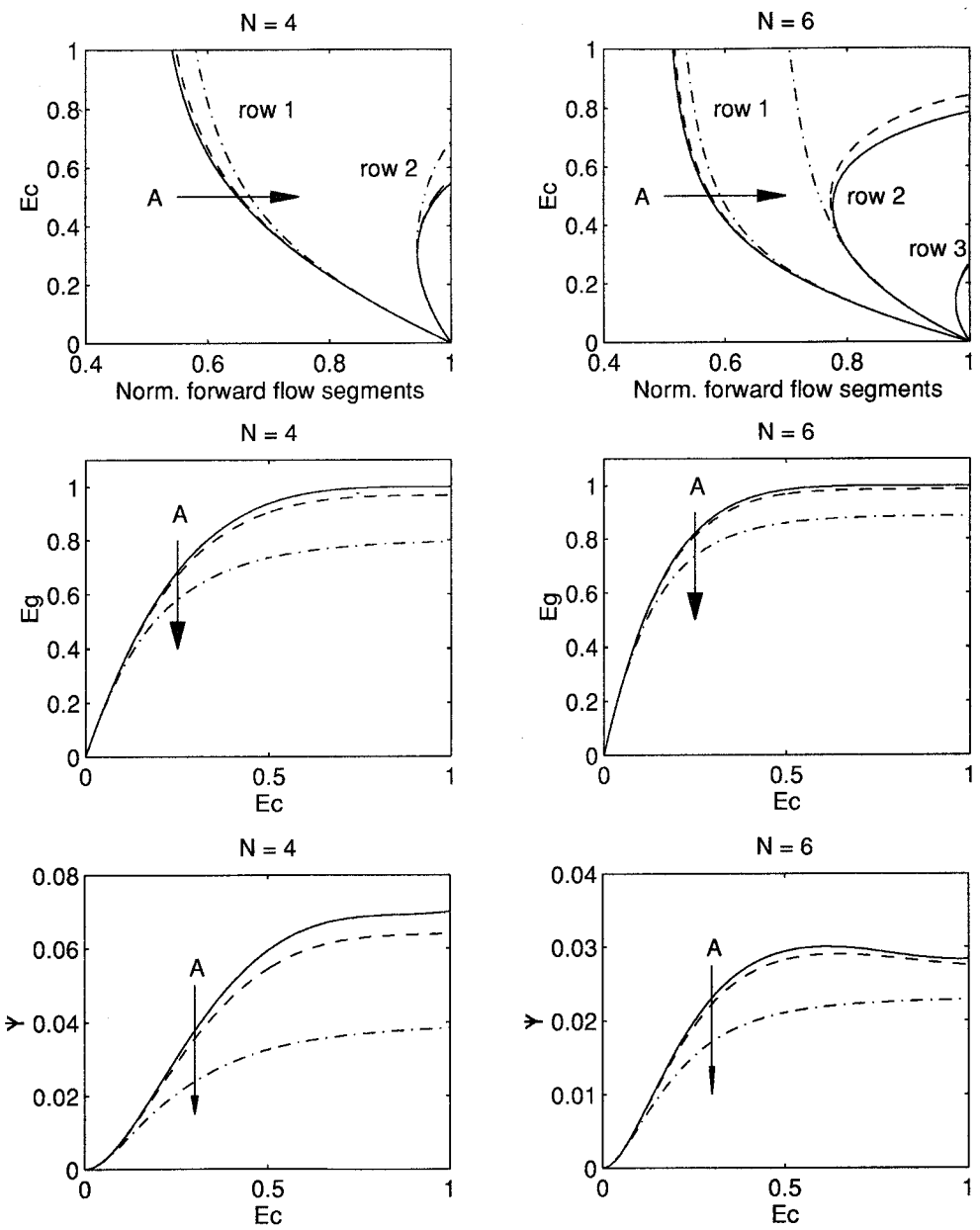

Fig. 2. Normalized forward flow segments, global effectiveness and normalized pressure drop between the inlet and the outlet plena versus the row effectiveness for A equal to 0 (solid), 1 (dash), and 10 (dot and dash) in four and six row condensers.

$$\frac{d\psi_n}{dy} = \begin{cases} +3\gamma_n\phi_n^2 & \text{for } \phi_n > 0 \\ -3\gamma_n\phi_n^2 & \text{for } \phi_n \le 0 \end{cases} \tag{16}$$

$$\theta_{sn} = 1 - A\psi_n \tag{17}$$

By solving the system composed of the differential Eqs. (15) and (16) and the auxiliary Eq. (17), the normalized vapor flow ϕ_n, internal depression ψ_n, and saturation temperature θ_{sn} are determined as a function of $\theta_n(y)$, $\phi_n(0)$, and $\psi_n(0)$. Assuming a uniform temperature distribution in the air entering the condenser, $\theta_1(y)$ is constant and equal to 0. The normalized temperature of the air crossing the second to the nth row is known as a function of the normalized saturation temperature and effectiveness patterns in the previous row. While $\psi_n(0)$ are zero for all rows, the initial normalized vapor flows $\phi_n(0)$ must be determined by

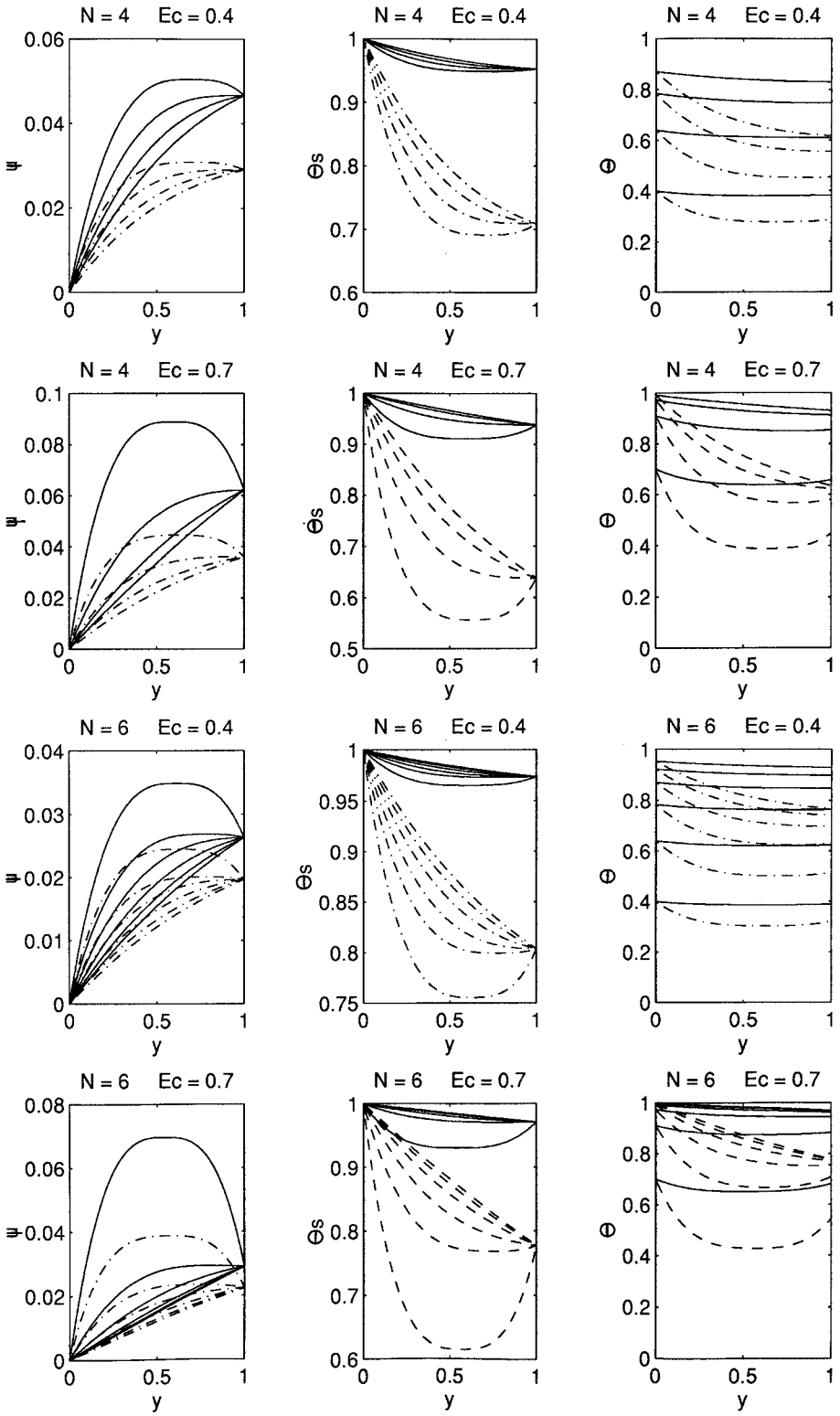

Fig. 3. Normalized depressions, vapor saturation temperatures and air temperature for A equal to 1 (solid) and 10 (dot and dash) in four and six row condensers. The highest depressions and the lowest temperatures concern the first row.

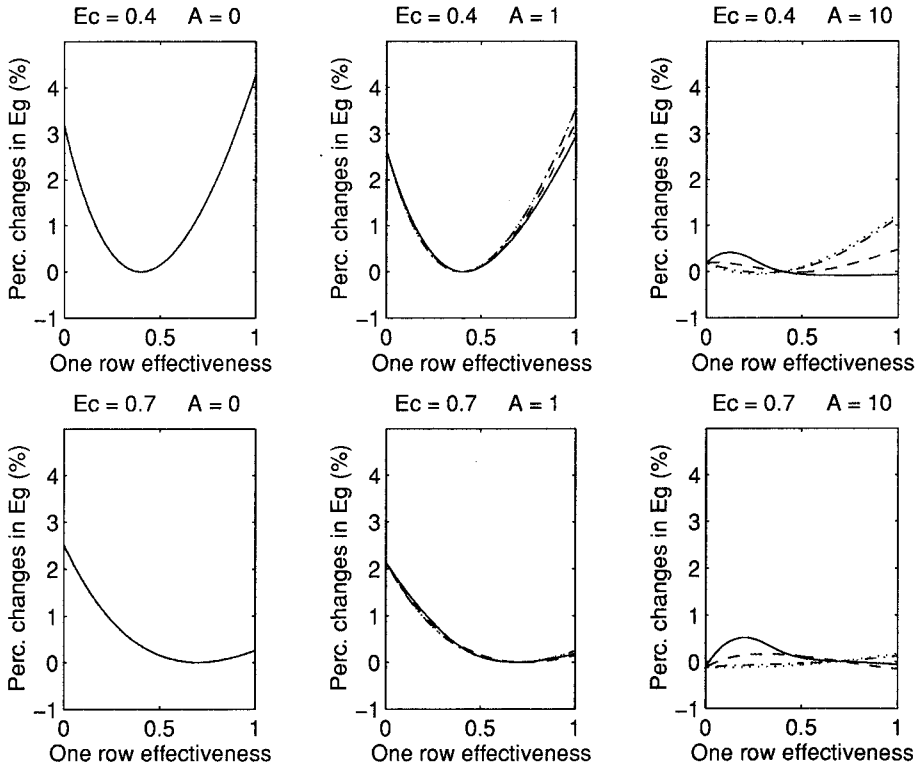

Fig. 4. Percentage changes in the global effectiveness obtained by varying the effectiveness of the first (solid), the second (dashes), the third (dots and dashes), and the fourth (dots) row for a given production cost.

imposing the following conditions:

$$\psi_n(1) = \psi_{n+1}(1) \quad \forall n = 1, 2, \ldots, N-1 \tag{18}$$

$$\sum_{1}^{N} \phi_n(1) = 0 \tag{19}$$

By solving the system composed of Eqs. (18) and (19) the vapor flow distribution into the condenser is determined. The solution can be easily found by utilizing the algorithm described in the appendix (Fig. A1).

After having determined the air temperature distribution along the tubes and among the rows, the global effectiveness of the condenser E_g can be calculated by referring to the saturation temperature at the beginning of the tubes and to the average output ($\bar{T}_{N+1}$) and input temperature of the air. Such a global effectiveness coincides with the average normalized output temperature of the air:

$$E_g = \frac{\bar{T}_{N+1} - T_1}{T_{sn}(0) - T_1} = \overline{\left(\frac{T_{N+1} - T_1}{T_{sn}(0) - T_1}\right)} = \bar{\theta}_{N+1} = \int_0^1 \omega_N(y)\theta_{N+1}(y)\,\mathrm{d}y \tag{20}$$

3. Results

The mathematical model presented in the previous section has been utilized to analyze the effect of changes along the tubes in the vapor saturation temperature, air velocity, and row effectiveness on the vapor distribution in condensers with four and six rows.

3.1. Changes in the saturation temperature

The effect of changes along the tubes in the saturation temperature due to the variations of the internal pressure has been investigated by assuming uniform air velocity ($\omega_n = 1$). The dependence of the saturation temperature on the pressure has been varied by consid-

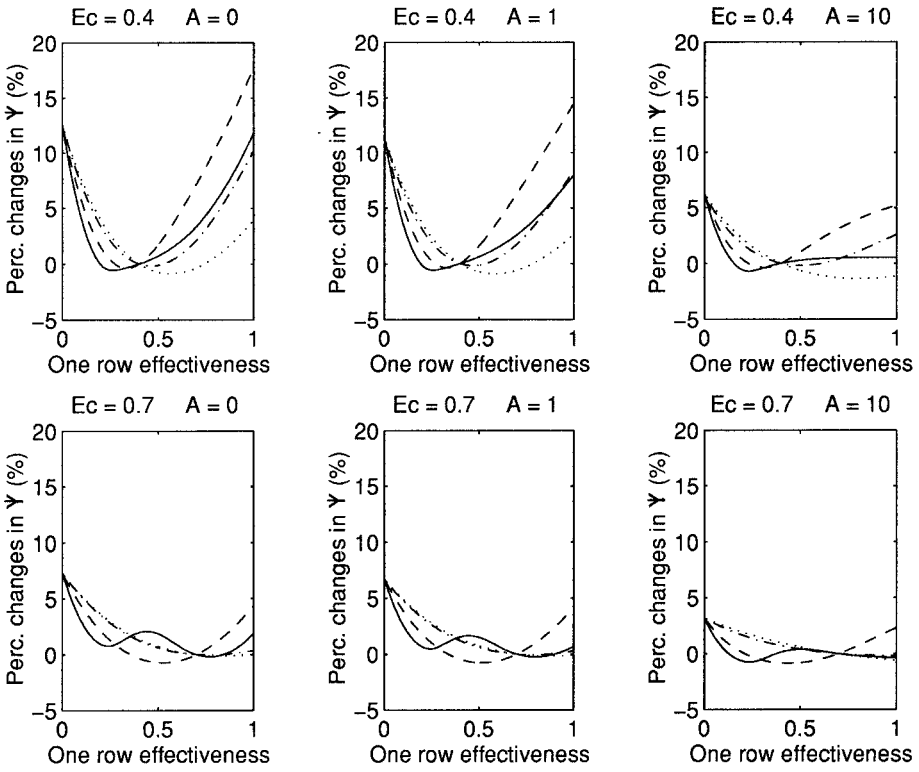

Fig. 5. Percentage changes in the pressure drop between the inlet and the outlet plena obtained by varying the effectiveness of the first (solid), the second (dashes), the third (dots and dashes), and the fourth (dots) row for a given production cost.

ering different values for parameter A. It must be remembered that this parameter is proportional to k_s, but also increases with the difference between the saturation temperature in the inlet plenum and the inlet air temperature, with the ratio between the heat capacity rate of the air and the latent heat of vaporization, and with the tube length.

In Fig. 2 the normalized forward flow segment lengths $\alpha_n = \alpha_n/L$, the global effectiveness E_g, and the normalized pressure drop $\Psi = \psi_n(1)$ between the inlet and the outlet plena are shown for condensers with four and six rows of the same effectiveness E_c in correspondence with three value (0, 1, 10) of parameter A. In the first two graphs, E_c is reported in the ordinate axis to let the forward flow segments extend in the horizontal direction as in Fig. 1. It is interesting to notice that when A is equal to 1 and to 10, no great difference can be observed for the four row condenser in the normalized forward flow segments with respect to the case of A equal to zero (isothermal condensation). In the six row condenser, higher variations of the saturation temperature can induce back flow in one more row. When the row effectiveness is high, in fact, while back flow only occurs in the first row for A equal to 0 and 1, it also occurs in the second row for A equal to 10. Moreover, in both condensers the normalized forward flow segments tend to equalize when parameter A increases. Lastly, it is evident that E_g and Ψ are more sensitive to variations in the saturation temperature in the four row than in the six row condenser.

It must be noticed that when parameter A is high, the saturation temperature assumes lower values inside the tubes. As a results, the vapor condensation rate, the vapor flows and the pressure changes are reduced. In particular, this occurs in the first rows where pressure and saturation temperature changes are higher. Therefore, when parameter A is high, the vapor condensation rate less noticeably changes among the rows and the forward flow segment length are more comparable.

In Fig. 3 the normalized depressions ψ_n, saturation temperatures θ_{sn}, and air temperatures θ_n are shown in correspondence with two values of A (1 and 10) and with a low (0.4) and a high (0.7) value of the row effectiveness E_c (the same for all rows). Higher changes along the tubes can be observed for all variables when the row effectiveness is higher and the number of rows smaller. Higher changes in the air and vapor saturation temperature, in fact, are caused by great variations of the pressure. These are induced by high vapor condensation rates and consequent high vapor flows.

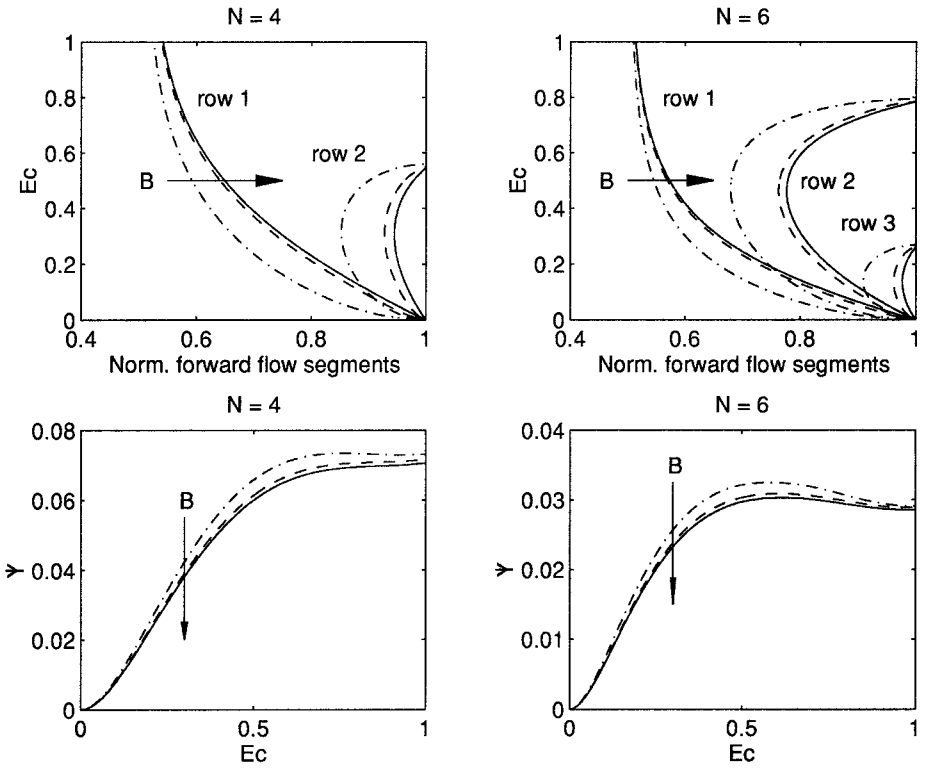

Fig. 6. Normalized forward flow segments and normalized pressure drop between the inlet and the outlet plena vs the row effectiveness for A and C equal to 0, and B equal to 200 (solid), 20 (dashes), and 2 (dots and dashes) in four and six row condensers.

Therefore, when the row effectiveness is high, larger changes in all variable are evident. Moreover, when the number of row is low, the pressure drop between the ends of the last row is higher, since the vapor back flow never occurs and the condensation rate is higher. As a consequence, pressure changes also are larger in the previous rows.

For a four row condenser, Figs. 4 and 5 show the percentage changes in the global effectiveness and in the normalized pressure drop between the inlet and the outlet plena obtained by varying the effectiveness of one row and letting that of the others be equal to a common value E_c. Changes are calculated referring to the global effectiveness of a reference condenser with the effectiveness of all rows equal to the average of the row effectiveness of the condenser where the effectiveness of one row is varied. The study of these changes is interesting if the production costs of the condenser can be assumed as depending on the average of the row effectivenesses [7]. It is evident that the relative increase of the global effectiveness, predicted for isothermal condensation [7] in correspondence with the reduction of the effectiveness of one row, becomes very little when A is high. Moreover, when A is not zero, variations of the effectiveness of each row produce different effects, while changes in the global effectiveness do not depend on the row whose effectiveness is varied for isothermal condensation. Lastly, when A increases, reductions of the normalized pressure drop between the inlet and the outlet plena occur in a larger domain than for isothermal condensation.

3.2. Changes in the air velocity

The effect of changes along the tubes in the air velocity has been investigated by assuming constant saturation temperature ($A = 0$). The following pattern has been assigned to the air velocity:

$$\omega_n(y) = \frac{B+1}{B}(1-|2y-1|^B) \tag{21}$$

For B ranging from 2 to ∞, the velocity profile varies from the parabolic to the flat shape. Changes in the air velocity can influence the row effectiveness in different manner. For an air column crossing an infinitesimal segment of a row, the local value of the row effectiveness increases with the global coefficient of the heat transfer between the vapor and the air, and decreases with the heat capacity rate of the air column [2]. Since both the global heat transfer coefficient and the heat

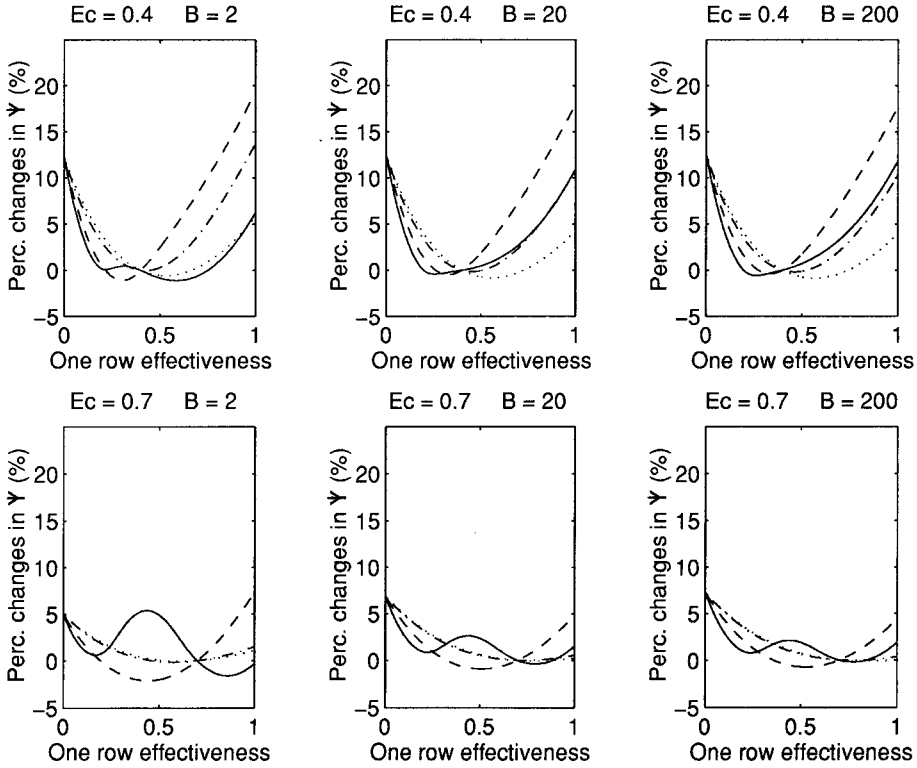

Fig. 7. Percentage changes in the pressure drop between the inlet and the outlet plena obtained by varying the average effectiveness of the first (solid), the second (dashes), the third (dots and dashes), and the fourth (dots) row for a given production cost and for A and C equal to 0.

capacity rate increase with the air velocity in different manner, the row effectiveness can increase or decrease depending on the working conditions. In an experimental condenser composed of four rows of horizontal glass tubes, for example, it has been observed [12] that, when the global air flow rate is lower, the row effectiveness increases with the air velocity along the tubes. An opposite dependence has been observed in correspondence with higher global air flow rates. By linearizing the dependence of the row effectiveness on the air velocity along the tubes, the following relationship can be written:

$$E_n(y) = \hat{E}_n\{1 + C[\omega_n(y) - 1]\} \tag{22}$$

where $\hat{E}_n$ is the average value of $E_n(y)$ for y ranging between 0 and 1. Parameter C can be positive or negative depending on the working conditions.

The direct effect of changes in the air velocity on the vapor distribution has been first investigated by assuming parameter C equal to 0 and assigning the same velocity profile to the air crossing each row. Under these conditions, the normalized forward flow lengths α_n and the normalized pressure drop Ψ between the inlet and the outlet plena are shown in Fig. 6 for condensers with four and six rows of the same effectiveness E_c in correspondence of three value (2, 20, 200) of parameter B. It is evident that the parabolic profile ($B = 2$) causes the shortest forward flow segments and the highest pressure drops between the inlet and outlet plena. Under the same conditions of Fig. 6, parameter B does not influence the global effectiveness, since the air temperature does not change along the tubes.

For a given production cost assumed as depending on the average of the row effectivenesses, Fig. 7 shows the percentage changes in the normalized pressure drop between the inlet and the outlet plena obtained by varying the effectiveness of one row and letting that of the others be equal to a common value E_c in a four row condenser. Parameter C has still been assumed equal to 0. It can be observed that, when the velocity profile is parabolic, to sensibly reduce the pressure drop, the effectiveness of the second row can be decreased, while that of the first row must be increased. On the contrary, when the velocity profile is nearly flat ($B = 200$), the pressure drop can not be sensibly reduced by acting on the effectiveness of the condenser rows. It must be noticed that the effectiveness of the condenser rows can be increased by enhancing the heat transfer between the vapor and the air, utilizing, for example, corrugated or finned tubes.

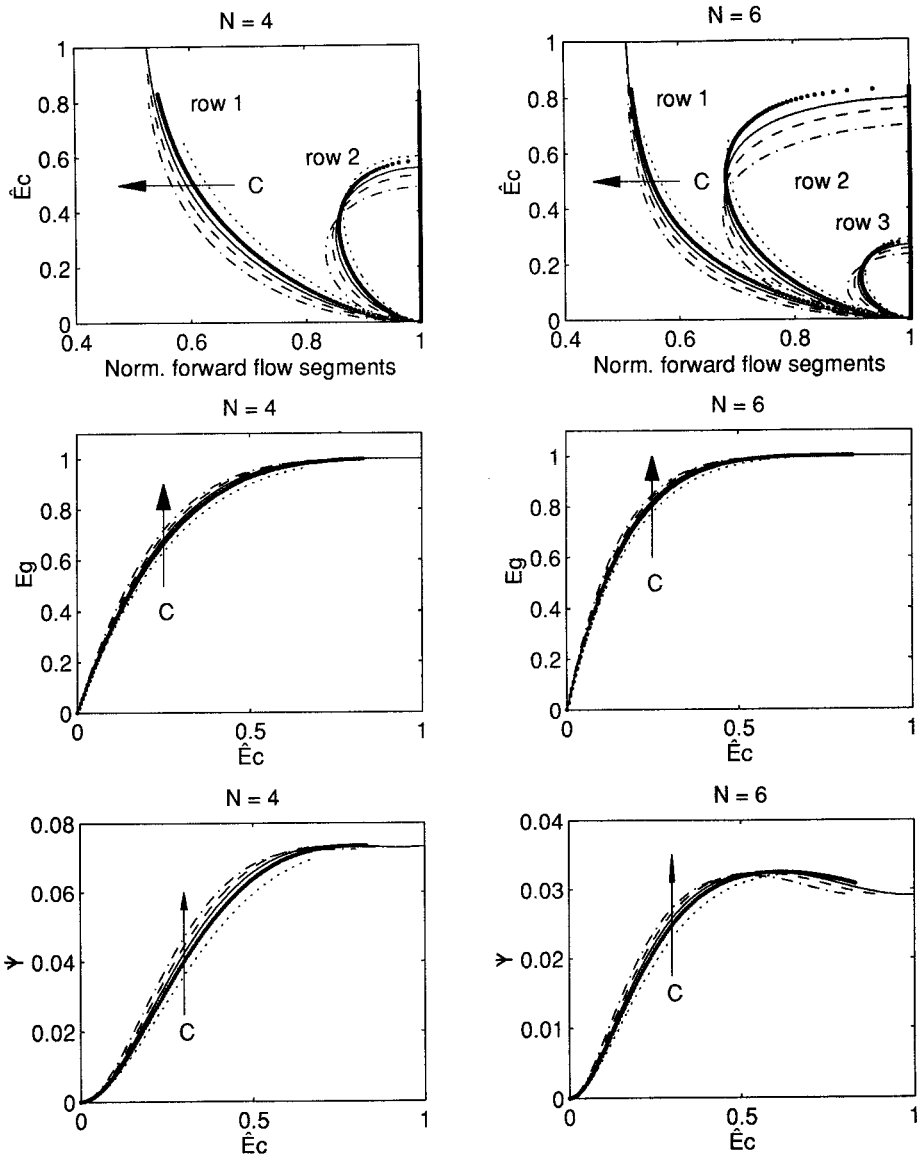

Fig. 8. Normalized forward flow segments, global effectiveness and normalized pressure drop between the inlet and the outlet plena versus the row effectiveness for A equal to 0, B equal to 2, and C equal to −0.5 (thin dots), −0.2 (thick dots), 0 (solid), 0.2 (dashes), and 0.5 (dots and dashes) in four and six row condensers.

To study the effect of changes in the row effectiveness due to the variations of the air velocity along the tubes, a parabolic velocity profile has been assumed ($B = 2$). Under this condition, the normalized forward flow lengths α_n, the global effectiveness E_g, and the normalized pressure drop Ψ between the inlet and the outlet plena are shown in Fig. 8 for condensers with four and six rows of the same average effectiveness $\hat{E}_c$ in correspondence of five values (−0.5, −0.2, 0, 0.2, 0.5) of parameter C. As in graphs of the next figures, points corresponding to physically consistent cases ($\max_x E_n(x) \leq 1$) are only reported. It is evident that the more the row effectiveness locally increases with the air velocity, the shorter the forward flow segment is in the first row. The same phenomenon only occurs in the other rows when $\hat{E}_c$ is low, while the opposite phenomenon occurs in the opposite case. Moreover, an increasing dependence of the row effectiveness on the air velocity always results in an increase in the global effectiveness, while influence the pressure drop in a different way depending on the value of $\hat{E}_c$.

For a given production cost assumed as depending on the average of the average row effectivenesses, Figs. 9 and 10 show the percentage changes in the global

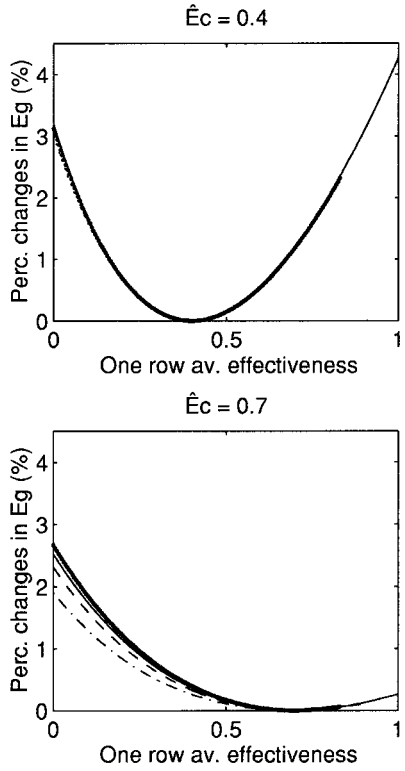

Fig. 9. Percentage changes in the global effectiveness obtained by varying the average effectiveness of the first (solid), the second (dashes), the third (dots and dashes), and the fourth (dots) row for a given production cost and for A equal to 0 and B equal to 2.

effectiveness and in the normalized pressure drop between the inlet and the outlet plena obtained by varying the average effectiveness of one row and letting that of the others be equal to a common value $\hat{E}_c$ in a four row condenser. A parabolic velocity profile has still been assumed. It can be observed that, when $\hat{E}_c$ is low parameter C influences the global effectiveness very few. On the contrary, when $\hat{E}_c$ is high, the relative increments in the global effectiveness are noticeably reduced in correspondence with positive values of parameter C. Moreover, positive values of parameter C increase the relative decrements, which can be obtained in the pressure drop by acting on the effectiveness of the first and second row, when $\hat{E}_c$ is low, and decrease them when $\hat{E}_c$ is high.

4. Conclusions

The proposed mathematical model allows the vapor distribution in single-pass, multiple-row, cross-flow, air-cooled condensers to be determined. The effect of pressure induced changes in the vapor saturation temperature, disuniformities in the air velocity, and variations along the tubes in the row effectiveness are taken into account. The model can be utilized to analyze the performances of condensers with as high a number of rows as desired with different effectiveness and friction factor.

The results obtained demonstrate that changes in the saturation temperature due to pressure variations along the tubes reduce the global effectiveness with respect to the case of isothermal condensation and can enhance vapor back flow phenomena (Table 1). In particular, in the studied cases, changes in the saturation temperature tend to lengthen the forward flow segment of the first row and shorten those of the others. Moreover, in a condenser with many rows, the number of rows where back flow occurs can be increased due to changes in the saturation temperature. These changes also reduce the convenience of decreasing the effectiveness of one row to increase the global effectiveness for given condenser production costs assumed as depending on the average of the row effectiveness [5].

Disuniformities in the air velocity enhance back flow phenomena reducing the length of the forward flow segments in the rows where back flow occur. They also increase the pressure drop between the inlet and the outlet plena and noticeably modify the effect of variations of the average effectiveness of one row for a given production cost.

For given average row effectivenesses, local changes in the row effectiveness induced by the velocity profile affect the length of the forward flow segments. In particular, the heat capacity rate of the air and the global

Table 1
Effect of increases in parameters A, B and C in correspondence of low (L) or high (H) values of the row effectiveness E_c: I—increases, D—decreases, NC—no change

Increasing parameter	E_c	E_g	Ψ	α_1	$\alpha_2 \ldots \alpha_N$	Back flow row number
A	L/H	D	D	I	D	I
B	L/H	NC	D	I	I	NC
C	L	I	I	D	D	I
C	H	I	D	D	I	D

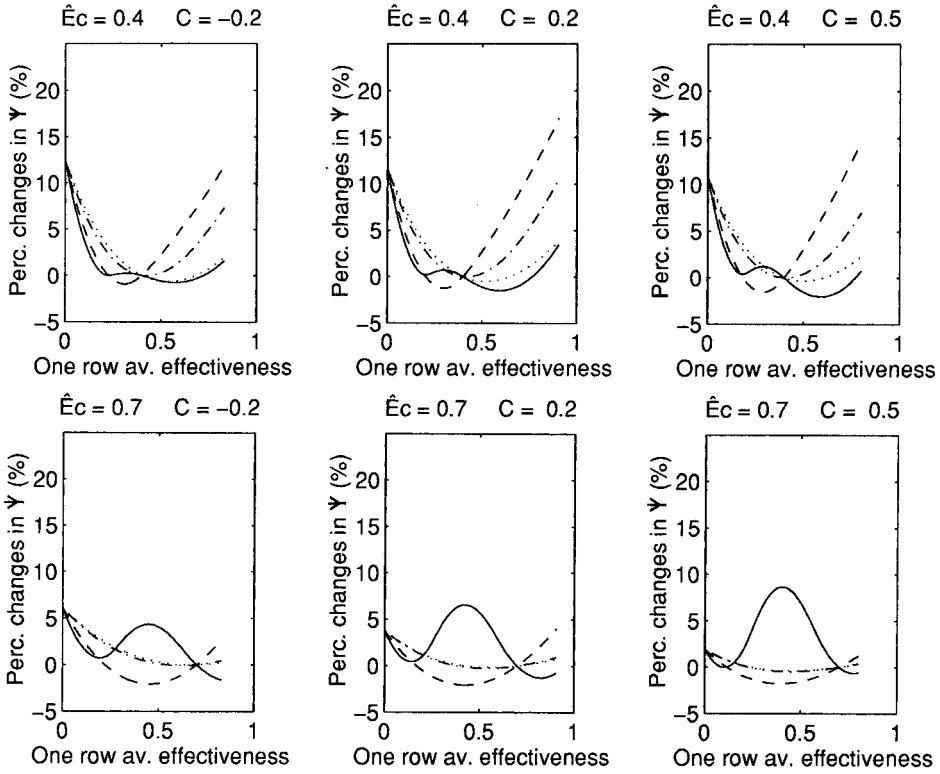

Fig. 10. Percentage changes in the pressure drop between the inlet and the outlet plena obtained by varying the average effectiveness of the first (solid), the second (dashes), the third (dots and dashes), and the fourth (dots) row for a given production cost and for A equal to 0 and B equal to 2.

coefficient of the heat transfer between the vapor and the air determine whether or not the forward flow segment are enlarged or decreased. Changes in the row effectiveness shortening the forward flow segments also decrease the number of rows where back flow occurs, slightly increase the global effectiveness, and, when the number of row is high, can reduce the pressure drop between the inlet and outlet plena. On the other hand, they reduce the convenience of decreasing the effectiveness of one row to increase the global effectiveness for given condenser production costs.

Appendix

The solution algorithm (Fig. A1) for the system composed of Eqs. (18) and (19) starts by setting the minimum and the maximum values which $\phi_1(0)$ can assume:

$$\phi_{01\,\min} = 0 \quad \phi_{01\,\max} = 1 + (N-1)\frac{1}{2} = \frac{N+1}{2} \tag{23}$$

The maximum value has been calculated referring to the ideal case where E_n is equal to 1, θ_{sn} to 1, θ_n to 0, and back flow occurs in the second to nth rows. In this case, back flow can not occur for a length larger than $L/2$ [7]. In the case corresponding to the above described mathematical model, θ_n can not be zero for all rows and the normalized vapor flow at the beginning of the first row results in being less than $\phi_{01\max}$.

The minimum and maximum values will be iteratively updated until their difference becomes less than a tolerance factor ϵ_ϕ. After having set the initial values for $\phi_{01\,\min}$ and $\phi_{01\max}$, an attempt value for $\phi_1(0)$ can be calculated:

$$\phi_{01a} = \frac{\phi_{01\,\min} + \phi_{01\,\max}}{2} \tag{24}$$

By numerically integrating system (15)–(17) for $\phi_1(0)$ equal to ϕ_{01a}, the normalized depression $\psi_1(1)$ at the end of the first row is determined.

Afterward, initial minimum, maximum and attempt values for $\phi_2(0)$ are set in the same way as for $\phi_1(0)$, and the depression at the end of the second row $\psi_2(1)$ is consequently calculated. If $\psi_2(1)$ results in being less than $\psi_1(1)$, the attempt value ϕ_{02a} is too low. The minimum limit is therefore updated as follows:

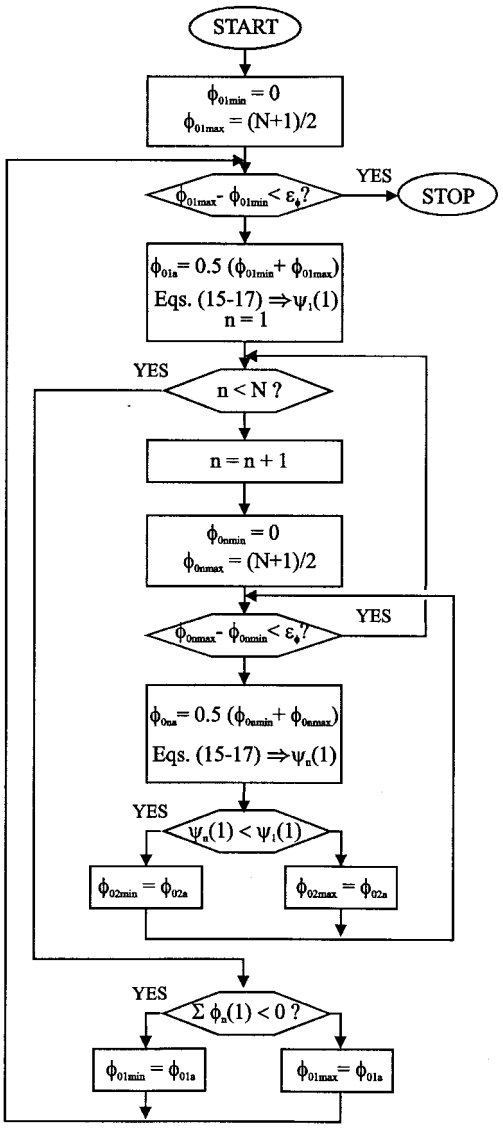

Fig. A1. Flow chart of the solution algorithm.

$$\phi_{02\ \min} = \phi_{02a} \tag{25}$$

Otherwise $[\psi_2(1) \geq \psi_1(1)]$ the maximum limit is updated:

$$\phi_{02\ \max} = \phi_{02a} \tag{26}$$

A new attempt value for $\phi_2(0)$ is then calculated as in Eq. (24) and the procedure is iterated until the difference between $\phi_{02\max}$ and $\phi_{02\ \min}$ becomes less than the tolerance factor ϵ_ϕ. In the same manner the vapor flow at the beginning of the tubes $\phi_n(0)$ is found for the other rows.

After having determined the vapor distribution which is consistent with the attempt value ϕ_{01a}, the sum of the vapor flows at the outlet end of the tubes is calculated. If this sum is negative, the attempt value ϕ_{01a} is too low. The minimum limit is therefore updated as follows:

$$\phi_{01\ \min} = \phi_{01a} \tag{27}$$

Otherwise, the maximum limit is updated:

$$\phi_{01\ \max} = \phi_{01a} \tag{28}$$

A new attempt value for $\phi_1(0)$ is then calculated and the procedure is iterated until the difference between $\phi_{01\max}$ and $\phi_{01\ \min}$ becomes less than the tolerance factor ϵ_ϕ.

References

[1] A.P. Fraas, Heat Exchanger Design, 2nd ed., Wiley, New York, 1989 Chap. 1.
[2] W.M. Kays, A.L. London, Compact Heat Exchangers, 3rd ed., McGraw-Hill, New York, 1984 Chap. 1.
[3] W.F. Berg, J.L. Berg, Flow patterns for isothermal condensation in one pass air cooled heat exchangers, Heat Transfer Eng. 1 (4) (1980) 21–31.
[4] G. Breber, J.W. Palen, J. Taborek, Study on noncondensable vapor accumulation in air-cooled condenser, Heat Exchangers 18 (1982) 263–268.
[5] G. Fabbri, Analysis of the effectiveness of single-pass air-cooled condensers, in: Proceedings of the Second European Thermal-Sciences Conference, Rome, Italy, May 29–31, 1996.
[6] G. Fabbri, Analysis of the noncondensable contaminant accumulation in single-pass air cooled condensers, Heat Transfer Eng. 18 (2) (1997) 50–60.
[7] G. Fabbri, Analysis of vapor back flow in single-pass air-cooled condensers, Int. J. Heat and Mass Transfer 40 (16) (1997) 3969–3979.
[8] T.F. Irvine Jr, P.E. Liley, Steam and Gas Tables with Computer Equations, Academic Press, Orlando, Florida, 1984.
[9] L.M. Schlager, M.B. Pate, A.E. Bergles, Heat transfer and pressure drop during evaporation and condensation of R22 in horizontal micro-finned tubes, Int. J. Refrig. 12 (1989) 6.
[10] D.L. Vrable, Condensation heat transfer inside horizontal tubes with internal axial fins, Ph.D. thesis, University of Michigan, 1974.
[11] N. Kaushik, N.Z. Azer, A general heat transfer correlation for condensation inside internally finned tubes, ASHRAE Trans. 94 (1) (1988) 261.
[12] G. Fabbri, S. Lazzari, S. Salvigni, P. Valdiserri, Analysis of condensation in single-pass cross-flow heat exchangers, in: Proceedings of the International Conference on Heat Exchangers for Sustainable Development, Lisbon, Portugal, June 15–18, 1998.